Materials Today Bio 24 (2024) 100938

Contents lists available at ScienceDirect

Materials Today Bio

journal homepage: www.journals.elsevier.com/materials-today-bio

Photoactive Poly-L-Lysine gel with resveratrol-magnesium metal polyphenol network: A promising strategy for preventing tracheal anastomotic complications following surgery

Yunxuan Jia [a,1], Jingfeng Shi [b,1], Bowen Ding [c,1], Liang Zhao [a], Ke Xu [a], Chuang Hu [e], Weijiao Xu [a], Anshun Zhu [d], Haitang Yang [a,**], Xiansong Wang [e,***], Feng Yao [a,d,*]

[a] Department of Thoracic Surgery, Shanghai Chest Hospital, Shanghai Jiao Tong University School of Medicine, Shanghai, 200030, China
[b] Department of Respiratory and Critical Care Medicine, No.2 People's Hospital of Fuyang City, Fuyang Infectious Disease Clinical College of Anhui Medical University, Fuyang, 236015, China
[c] Department of Pathology, Shanghai Chest Hospital, Shanghai Jiao Tong University School of Medicine, Shanghai, 200030, China
[d] Wenzhou Medical University, Wenzhou, 325015, China
[e] Department of Thoracic Surgery, Shanghai Key Laboratory of Tissue Engineering, Shanghai Ninth People's Hospital, Shanghai Jiao Tong University School of Medicine, Shanghai, 200011, China

ARTICLE INFO

Keywords:
Tracheal resection
Anastomotic complications
Resveratrol
Metal-polyphenol networks
Stenosis
Hydrogels

ABSTRACT

Postoperative complications at the anastomosis site following tracheal resection are a prevalent and substantial concern. However, most existing solutions primarily focus on managing symptoms, with limited attention given to proactively preventing the underlying pathological processes. To address this challenge, we conducted a drug screening focusing on clinically-relevant polyphenolic compounds, given the growing interest in polyphenolic compounds for their potential role in tissue repair during wound healing. This screening led to the identification of resveratrol as the most promising candidate for mitigating tracheal complications, as it exhibited the most significant efficacy in enhancing the expression of vascular endothelial growth factor (VEGF) while concurrently suppressing the pivotal fibrosis factor: transforming growth factor-beta 1 (TGF-β1), showcasing its robust potential in addressing these issues. Building upon this discovery, we further developed an innovative photosensitive poly-L-lysine gel integrated with a resveratrol-magnesium metal polyphenol network (MPN), named Res-Mg/PL-MA. This design allows for the enables sustained release of resveratrol and synergistically enhances the expression of VEGF and also promotes resistance to tensile forces, aided by magnesium ions, in an anastomotic tracheal fistula animal models. Moreover, the combination of resveratrol and poly-L-lysine hydrogel effectively inhibits bacteria, reduces local expression of key inflammatory factors, and induces polarization of macrophages toward an anti-inflammatory phenotype, as well as inhibits TGF-β1, consequently decreasing collagen production levels in an animal model of post-tracheal resection. In summary, our novel Res-Mg/PL-MA hydrogel, through antibacterial, anti-inflammatory, and pro-vascularization mechanisms, effectively prevents complications at tracheal anastomosis, offering significant promise for translational applications in patients undergoing tracheal surgeries.

* Corresponding author.Department of Thoracic Surgery, Shanghai Chest Hospital, Shanghai Jiao Tong University School of Medicine; West Huaihai 241, Shanghai, 200030, China.
** Corresponding author. Department of Thoracic Surgery, Shanghai Chest Hospital, Shanghai Jiao Tong University School of Medicine; West Huaihai 241, Shanghai, 200030, China.
*** Corresponding author. Department of Thoracic Surgery, Shanghai Key Laboratory of Tissue Engineering, Shanghai Ninth People's Hospital, Shanghai Jiao Tong University School of Medicine, Zhizaoju 639, Shanghai, 200011, China.
E-mail addresses: haitang.yang@shsmu.edu.cn (H. Yang), wonderluis@sjtu.edu.cn (X. Wang), yaofeng@shsmu.edu.cn (F. Yao).
[1] Contributed equally.

https://doi.org/10.1016/j.mtbio.2023.100938
Received 27 October 2023; Received in revised form 19 December 2023; Accepted 28 December 2023
Available online 29 December 2023

1. Introduction

Tracheal surgery plays a vital role in addressing a range of medical conditions, including tracheal stenosis following intubation, laryngotracheal tumors, tracheoesophageal fistulas, and idiopathic laryngotracheal stenosis. One of the most pressing issues following such surgeries is the occurrence of anastomotic complications, which pose a considerable risk to patients.

In the early postoperative period, the predominant challenge faced is the overgrowth of granulomatous tissue [1,2]. While granulation tissue is essential for wound healing, its excessive and persistent proliferation can lead to airway blockages, subsequent scarring, and ultimately, stenosis [3]. Furthermore, minor dehiscence, often manifested as local infection and the formation of small fistulas, is a common occurrence in clinical practice [4]. The current therapeutic strategies, primarily centered around bronchoscopic techniques, still face persistent risks of recurrent granulomas and airway stenosis [3,5–7]. This suggests that current solutions might not be addressing the core of the problem.

The root causes of anastomotic complications can be traced to excessive local tension, chronic inflammation due to foreign body stimuli, and insufficient blood supply leading to poor healing [8]. The trachea's inherent exposure to the external environment accentuates the importance of preventing infections at the anastomotic site. Infections, when driven by inflammation, can boost fibroblast activity, accelerate granulation tissue growth, and subsequently lead to scar formation and tracheal narrowing [9,10]. Furthermore, due to the compromised blood supply post-tracheal surgery and the trachea's inherent lack of vascularization, there's an emphasis on the need for promoting microcirculation to avoid anastomotic dehiscence. Therefore, the pivotal strategy for mitigating tracheal anastomotic complications hinges on proficiently managing infections, attenuating overactive inflammatory cascades, and fostering microvascular angiogenesis.

Following tracheal surgery, intravenous antibiotic administration remains the primary clinical method for infection prevention. However, owing to surgical-induced blood supply disruption and the inherent vascular nature of the trachea, localized infections can sometimes be challenging to rapidly control. Although antibiotic inhalation is another option, its application is restricted due to significant irritation to the trachea [11]. Consequently, the local application of antimicrobial materials has emerged as a promising therapeutic strategy [12]. Among the existing antimicrobial dressings, poly-L-lysine gel has garnered widespread attention due to its potent drug delivery capabilities and its inherent broad-spectrum antibacterial properties, making it an excellent candidate for the development of multifunctional hydrogel dressings [13].

In addition to the inflammation caused by infections, chronic inflammation resulting from mechanical tension and foreign body irritation can also lead to granulation tissue proliferation and scar constriction. Clinically, the usual approach to address this challenge involves local steroid injections under bronchoscopy; however, this often fails to yield the expected results. Among the current anti-inflammatory agents, our previous research has found that polyphenolic compounds exhibit strong effects in suppressing inflammatory factors and promoting macrophage phenotype polarization [14–17]. Through screening potential candidate molecules, resveratrol emerged as the most promising agent for its anti-fibrotic properties and its ability to promote tissue repair. However, the clinical application of resveratrol is limited due to its poor water solubility and low tissue bioavailability. The metal-polyphenol network has recently emerged as an excellent strategy to overcome these challenges. With its high porosity and flexibility, it can encapsulate and release drugs in a controlled manner. Furthermore, when the drug binds with metal ions to form a polymer, its solubility and stability are enhanced, making local application feasible.

Building on this research, we constructed a metal-polyphenol network using magnesium ions and resveratrol, and integrated it into a photosensitive poly L-lysine gel. This resulted in a novel hydrogel named Res-Mg/PL-MA. Our design aims to harness the combined strengths of resveratrol, magnesium ions, and PL-MA to address the three major challenges associated with tracheal anastomosis: infection prevention, attenuation of overactive inflammatory responses, and promotion of microvascular angiogenesis (see Scheme 1).

2. Results

2.1. In vitro drug screening

Potent polyphenolic compounds that promote angiogenesis and inhibit fibrosis were identified, selecting six clinically significant compounds known to aid in skin wound healing. These compounds are tannic acid, gallic acid, curcumin, caffeic acid, chlorogenic acid, and resveratrol.

In the drug screening process, rabbit-derived tracheal fibroblasts were isolated and exposed to these polyphenolic compounds for a duration of 10 h, using concentrations commonly employed in related studies. The expression levels of transforming growth factor-beta (TGF-β1) and vascular endothelial growth factor (VEGF) in these cells were evaluated using quantitative real-time polymerase chain reaction (qRT-PCR) (Fig. 1a).

The results indicated that among the six polyphenolic compounds, all of them, with the exception of caffeic acid, demonstrated the ability to downregulate TGF-β1 expression and upregulate VEGF expression (Fig. 1b and c). In particular, resveratrol (Res) and gallic acid (GA) exhibited the most robust inhibitory effects on TGF-β1. When it comes to the upregulation of VEGF levels, resveratrol exhibited the highest potency. Consequently, resveratrol emerges as the most promising candidate for addressing our research objectives. It's worth noting that resveratrol is approved by the United States Food and Drug Administration (U.S. FDA) for use as a dietary supplement and additive and also widely employed in scarless skin repair, rendering it highly relevant for clinical applications.

2.2. synthesis and characterization of Res-Mg and Res-Mg/PL-MA

To characterize the structure of our Res-Mg, we utilized scanning electron microscopy, revealing a spherical configuration with a diameter of approximately 10 μm (Fig. 2a). Characteristic peaks from X-ray diffraction experiments further confirmed its successful synthesis (Fig. 2b).

To investigate the potential sustained release of resveratrol, we immersed the Res-Mg/PL-MA hydrogel in PBS. Over time, we collected samples and quantified the release of resveratrol. The drug release curve revealed a gradual release of resveratrol from the Res-Mg/PL-MA hydrogel into the PBS. This release stabilized on the third day, with a total quantity maintained at 55.19 μM ± 3.63 μM (Fig. 2c). The sustained release curve demonstrates that the dual sustained-release system of Res-Mg/PLMA outperforms the other two single-release systems: Res-Mg and Res/PL-MA in terms of sustained release performance.

While PL-MA demonstrates good biocompatibility, the safety of the Res-Mg/PL-MA hydrogel requires further investigation under the scenario of tracheal anastomosis. To address this, we cultivated rabbit tracheal fibroblasts and the human airway epithelial cell line BEAS-2B in a medium containing Res-Mg/PL-MA for 72 h and assessed their cellular viability. The results showed no inhibition of the cell viability treated with these compounds at short- (72h) (Fig. 2d) and long-term (5 days) (Fig. 2e) time. To compare the differences in cell viability among colony clones, we conducted a quantitative analysis of their overall absorbance. The results indicated that varying concentrations of resveratrol did not significantly impact fibroblast and BEAS-2B cell viability (Fig. 2f). This demonstrates that Res-Mg/PL-MA has good biocompatibility in the tracheal tissue environment.

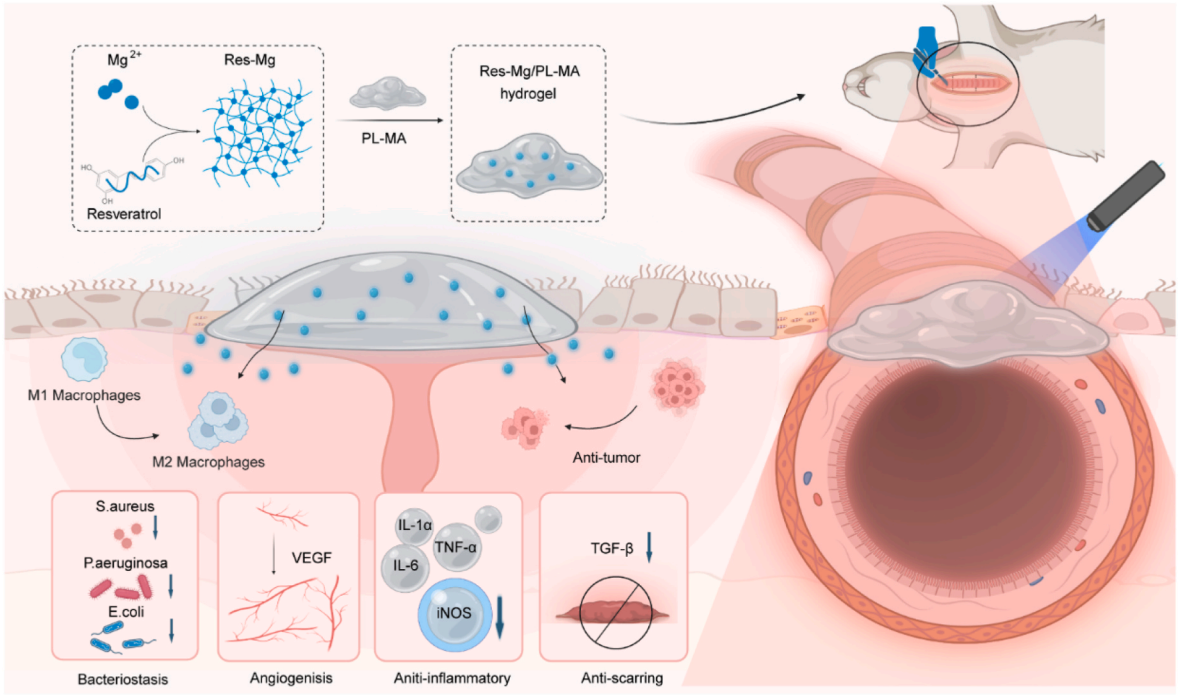

Scheme 1. Schematic illustration of the animal model construction and the molecular mechanism of the Res-Mg/PL-MA hydrogel.

2.3. Res-Mg/PL-MA possesses in vitro antibacterial activity

Given the trachea's exposure to the external environment and the common impairment of its blood supply during surgery, it becomes susceptible to bacterial infections after the operation. Three representative bacteria commonly responsible for airway infections were selected to evaluate the antibacterial activity of the Res-Mg/PL-MA hydrogel. These include *Staphylococcus aureus* (Gram-positive), *Escherichia coli* (Gram-negative), and *Pseudomonas aeruginosa*. The antibacterial tests were conducted using the disc diffusion method.

24 h after bacterial inoculation, photographs of all three clearly showed inhibition zones (Fig. 3). In all three bacterial strains, both the PL-MA group and the Res-Mg/PL-MA group showed significant differences in the diameter of the inhibition zone compared to the control group. The diameters of the zones for *Staphylococcus aureus*, *Pseudomonas aeruginosa*, and *Escherichia coli* in the Res-Mg/PL-MA were 3.61, 2.70, and 3.79 times that of the control group, respectively. This proves that Res-Mg/PL-MA possesses broad-spectrum antibacterial properties, effectively combating various airway bacterial infections.

2.4. Res-Mg/PL-MA enhances the anti-tension strength at the anastomotic sites

Reducing anastomotic tension following tracheal resection is vital in minimizing the risk of rupture or fistula post-surgery. In our next step, we investigated whether the Res-Mg/PL-MA hydrogel possessed anti-tension properties. To assess this, we established an animal model of tracheal segmental resection (Fig. 4a and b).

Our findings demonstrated that the Res-Mg/PL-MA hydrogel significantly alleviated anastomotic tension when compared to the Res-Mg or PL-MA hydrogel used individually (Fig. 4c). Notably, Res-Mg/PL-MA provided the highest maximum tensile strength in comparison to Res-Mg or PL-MA hydrogel alone (Fig. 4d). These results indicate that our Res-Mg/PL-MA hydrogel enhances the mechanical strength of the tracheal anastomotic site during the initial stages of healing.

2.5. Res-Mg/PL-MA inhibits granulation tissue formation at the anastomotic site

Subsequently, we conducted further investigations into the potential of Res-Mg/PL-MA in preventing granulation tissue proliferation and anastomotic stenosis at the junction, using the same animal models as before. After a 14-day period, samples were collected, revealing complete healing of the tracheae in all rabbits across the four groups. To gauge the extent of lumen narrowing, we used normal cartilage rings adjacent to the anastomotic site as reference points.

The results demonstrated a significant reduction in the narrowing ratio of the Res-Mg group and the Res-Mg/PL-MA group when compared to the untreated group, with the combination group (Res-Mg/PL-MA) exhibiting the least degree of lumen narrowing (Fig. 5a–c). This indicates that resveratrol effectively inhibits the occurrence of tracheal anastomotic narrowing, and through the controlled release of Res-Mg/PL-MA, its inhibitory effect on anastomotic narrowing is further enhanced.

The superiority of Res-Mg/PL-MA was further substantiated through histological examinations. H&E staining revealed that the thickness of granulation tissue in the Res-Mg/PL-MA group exhibited the most significant reduction in comparison to the other groups (Fig. 5b–d). Additionally, Masson's staining, which assessed collagen components, indicated that the collagen volume fraction (CVF) content was the lowest in the Res-Mg/PL-MA group (Fig. 5b–e). This further confirms that Res-Mg/PL-MA possesses the greatest efficacy in reducing the formation of granulation tissue at the tracheal anastomotic site.

At the molecular level, it was evident that the Res-Mg/PL-MA group exhibited a marked reduction in TGF-β1 expression. This reduction is particularly significant since TGF-β1 is typically acknowledged as a major contributor to the hyperplasia of granulomas and the development of stenosis (Fig. 5f). In summary, both animal models and *in vitro* experiments have demonstrated that Res-Mg/PL-MA effectively prevents granulation tissue proliferation and anastomotic stenosis in the trachea.

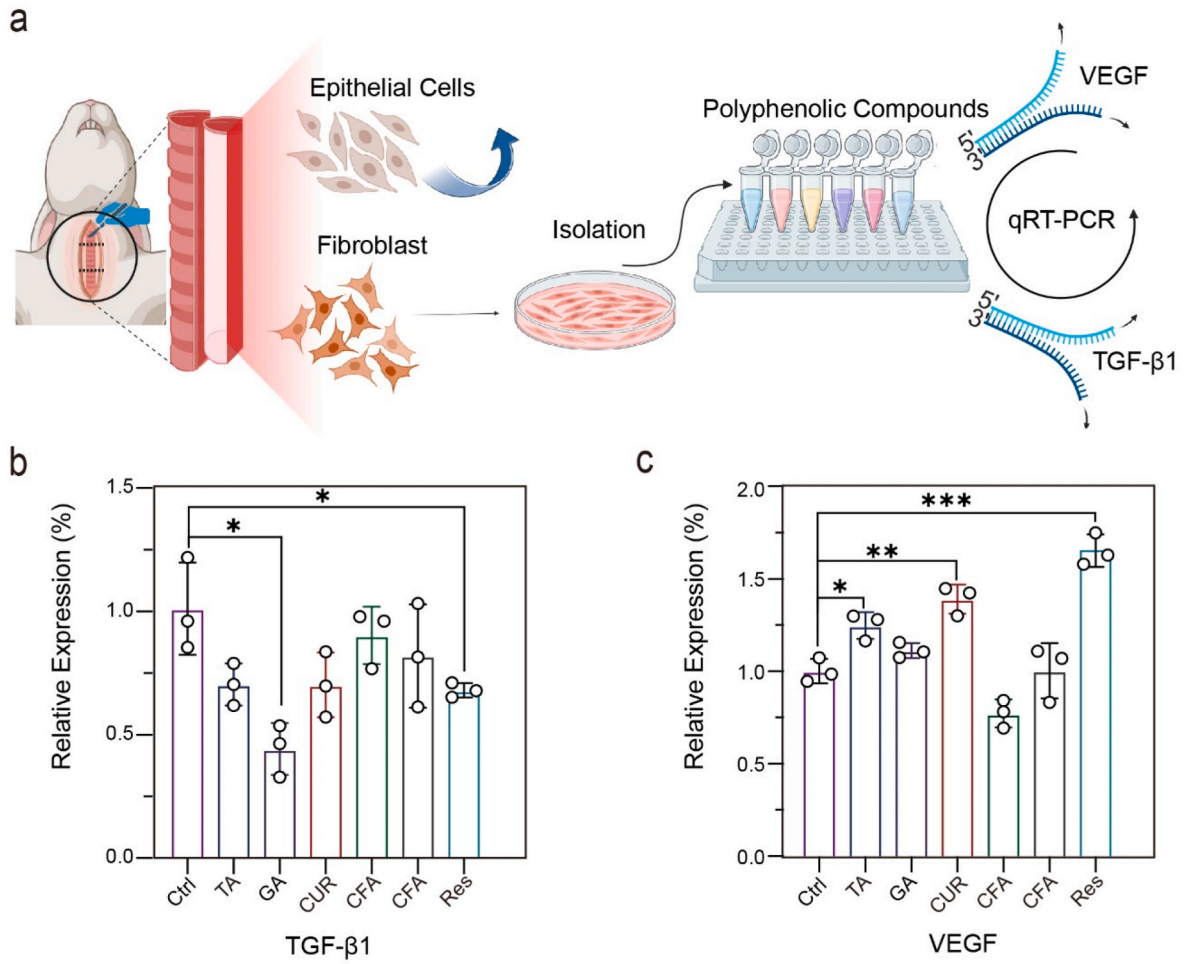

Fig. 1. a: Schematic illustration of drug screening. b, c: Relative qPCR expression levels of TGF-β1 and VEGF in cells treated with different drug concentrations (TA: tannic acid 25 μM, GA: gallic acid 100 μM, CUR: curcumin 5 μg/mL, CFA: caffeic acid 5 μM, CHA: chlorogenic acid 100 μg/mL, Res: resveratrol 50 μM). Statistics were calculated by Student's t-test. *p < 0.05, **p < 0.01, ***p < 0.001, ****p < 0.0001 unless otherwise indicated. Data are presented as mean ± standard deviation (SD).

2.6. Res-Mg/PL-MA exhibits the potency in repairing anastomotic fistula and promoting angiogenesis

Anastomotic fistula is a life-threatening complication that can occur after tracheal surgery. To further assess the effectiveness of Res-Mg/PL-MA in preventing or promoting the repair of anastomotic fistulas, we established a tracheal anastomotic fistula model (Fig. 6a and b).

Survival analysis revealed a significant improvement in the survival rate of rabbits in the groups treated with PL-MA gel, Res-Mg drug, and the combination of Res-Mg/PL-MA, as compared to the untreated group. Notably, the Res-Mg/PL-MA combination exhibited a synergistic effect when compared to the two single treatment groups (Fig. 6c). Rabbit deaths were primarily attributed to dyspnea, or in combination with infection. Upon examining gross specimens of the tracheal anastomotic sites at the endpoint (either upon death or the conclusion of the experiments) of each rabbit, it was evident that the rate of partial anastomotic separation in the RES and Res-Mg/PL-MA groups was significantly lower than that in the untreated group. The Res-Mg/PL-MA group, in particular, demonstrated the most effective prevention and repair of tracheal anastomotic fistulas (Fig. 6d).

Given the critical role of tracheal vasculature in anastomotic healing, we subsequently explored the potential impact of Res-Mg/PL-MA on microvascular formation. At the molecular level, qPCR demonstrated that Res-Mg/PL-MA markedly elevated the expression of VEGF compared to other treatment groups (Fig. 6e). Immunohistochemical staining for the vascular marker CD31 indicated the highest signal intensity in the Res-Mg/PL-MA group (Supplementary Fig. 1a). Quantitative analyses corroborated this observation, revealing a significantly greater proportion of CD31-positive cells in the Res-Mg/PL-MA group compared to others (Supplementary Fig. 1b). Additionally, utilizing alpha-smooth muscle actin(α-SMA) as a marker for myofibroblasts and vascular smooth muscle cells, the Res-Mg/PL-MA group also exhibited pronounced signal enhancement (Supplementary Fig. 1c). Collectively, these findings strongly suggest that Res-Mg/PL-MA is highly effective in promoting the healing and tissue vascularization of tracheal anastomotic sites.

2.7. Res-Mg/PL-MA has the strongest anti-inflammatory effect

Following the remarkable efficacy of Res-Mg/PL-MA in our animal model, we delved into the potential molecular mechanisms underlying tracheal complications. Given the central role of macrophage-induced inflammatory responses in tracheal surgery complications, the expression levels of primary inflammatory factors, notably IL-1α, IL-6, and TNF-α, were evaluated using qPCR. After treating mouse macrophages with extracts from PL-MA gel and Res-Mg/PL-MA overnight, data showed a significant reduction in the expression of these inflammatory markers (Fig. 7a–c).

Moreover, through flow cytometry analysis, we observed a significant increase in the expression of CD206, a marker for the M2 subtype of

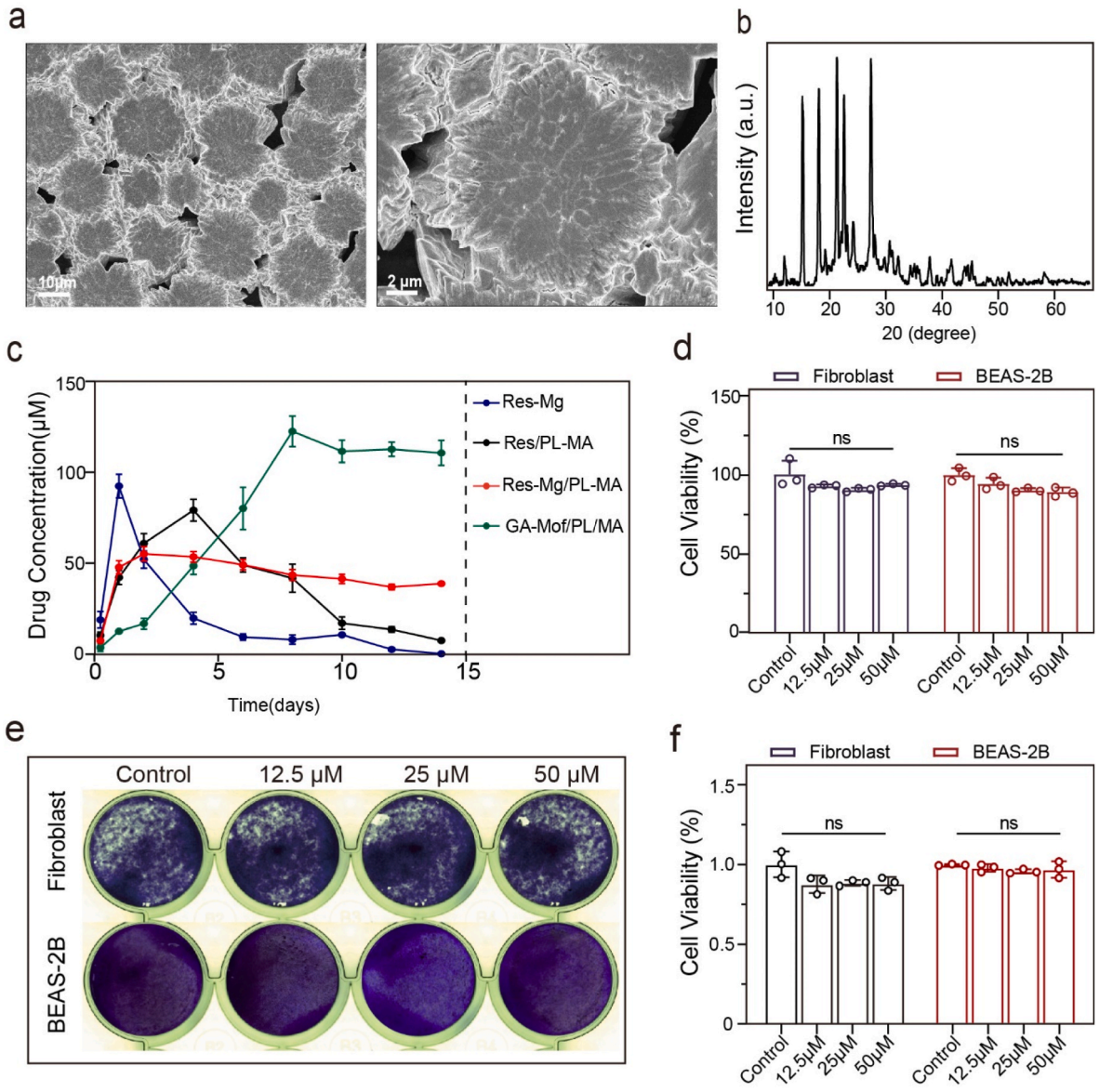

Fig. 2. a: Images of Res-Mg under low and high magnification in scanning electron microscopy (SEM). b: X-ray diffraction (XRD) spectrum of Res-Mg powder. c: Drug release curve of resveratrol from Res-Mg, Res/PL-MA and Res-Mg/PL-MA hydrogel in PBS. The drug release from GA-Mof/PL-MA serves as the positive control. d: Relative viability of BEAS-2B and rabbit fibroblasts post-treatment at various concentrations for 72 h. e, f: Colony-forming images (e) and quantitative analysis (f) of rabbit fibroblasts and BEAS-2B following treatment with different concentrations of resveratrol for 5 days. Statistics were calculated with Student's t-test. 'ns' represents no significant difference ($p > 0.05$). Data are presented as mean ± standard deviation (SD).

macrophages, in macrophage cells treated with Res-Mg and Res-Mg/PL-MA for 4, 8 and 24 h, compared to the group without resveratrol (Fig. 7d–g). The qPCR results also indicated a significant decrease in the expression of iNOS, a marker of the M1 subtype of macrophages (Fig. 7h). This indicates that Res-Mg/PL-MA plays a role in promoting the polarization of macrophages towards an anti-inflammatory phenotype. In summary, it was demonstrated that Res-Mg/PL-MA can significantly inhibit the inflammatory response induced by macrophages.

2.8. Res-Mg/PL-MA has antitumor effects

Tracheal malignancy is a strong indicator for surgical intervention, accounting for half of all cases requiring tracheal surgery. Consequently, we conducted experiments to investigate the potential inhibitory effects of resveratrol on airway tumors.

Cell viability assays (Fig. 8a) and colony formation tests (Fig. 8b) indicated that resveratrol significantly suppresses the growth of various non-small cell lung cancer (NSCLC) cell lines (A549, PC-9, and H1299), both in short-term and long-term evaluations [18]. Adenoid cystic carcinoma (ACC) is the predominant histological subtype in tracheal malignancies. Utilizing intraoperative samples from a patient who successfully underwent segmental tracheal resection due to ACC (Fig. 8c), a highly clinically relevant patient-derived organoid (PDO) model was established. Sequential imaging revealed that while the organoids in the control group exhibited normal growth over time, the organoids in the drug-treated group underwent apoptosis (Fig. 8d). Growth trajectories demonstrated a pronounced difference between the control and the drug-treated organoids (Fig. 8e). Additionally, ATPase cellular vitality assays highlighted a substantial reduction in the vitality of the organoid tumor cells post-resveratrol treatment (Fig. 8f). Cumulatively, these findings attest to the potent inhibitory effect of resveratrol on ACC PDO growth, suggesting that Res-Mg/PL-MA offers significant promise in addressing post-tracheal resection tumor remnants.

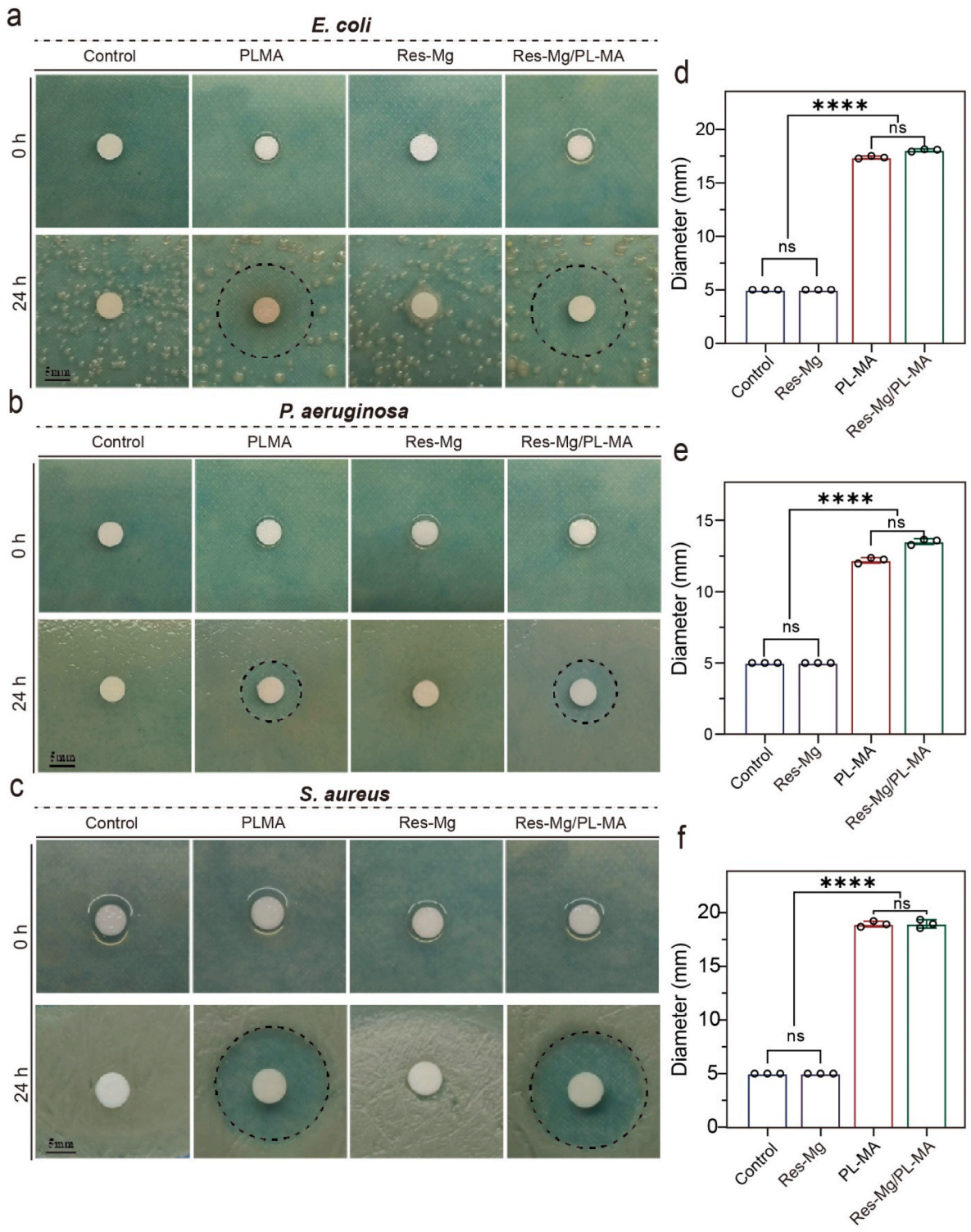

Fig. 3. a, b, c: Representative photos of the inhibition zones for various bacterial strains treated with the extracts of PL-MA, Res-Mg, and Res-Mg/PL-MA. d, e, f: Quantification of the inhibition zone diameters for each group. Statistics were calculated with Student's t-test. *$p < 0.05$, **$p < 0.01$, ***$p < 0.001$, ****$p < 0.0001$ unless otherwise indicated. Data are presented as mean ± standard deviation (SD).

3. Discussion

Addressing the challenges associated with complications arising from tracheal anastomoses represents a substantial obstacle for surgeons [3,19]. These complications may be attributed to a variety of factors, including the trachea's unique anatomy, which is characterized by poor blood supply, local tension following a segment resection, its exposure to the external environment, and foreign body reactions stemming from surgical sutures. Current approaches predominantly concentrate on optimizing intraoperative surgical techniques and postoperative symptom management, frequently neglecting the underlying pathophysiological mechanisms responsible for inciting anastomotic complications. Our study represents the first attempt to tackle the issue by examining the pathological causes of tracheal anastomotic complications.

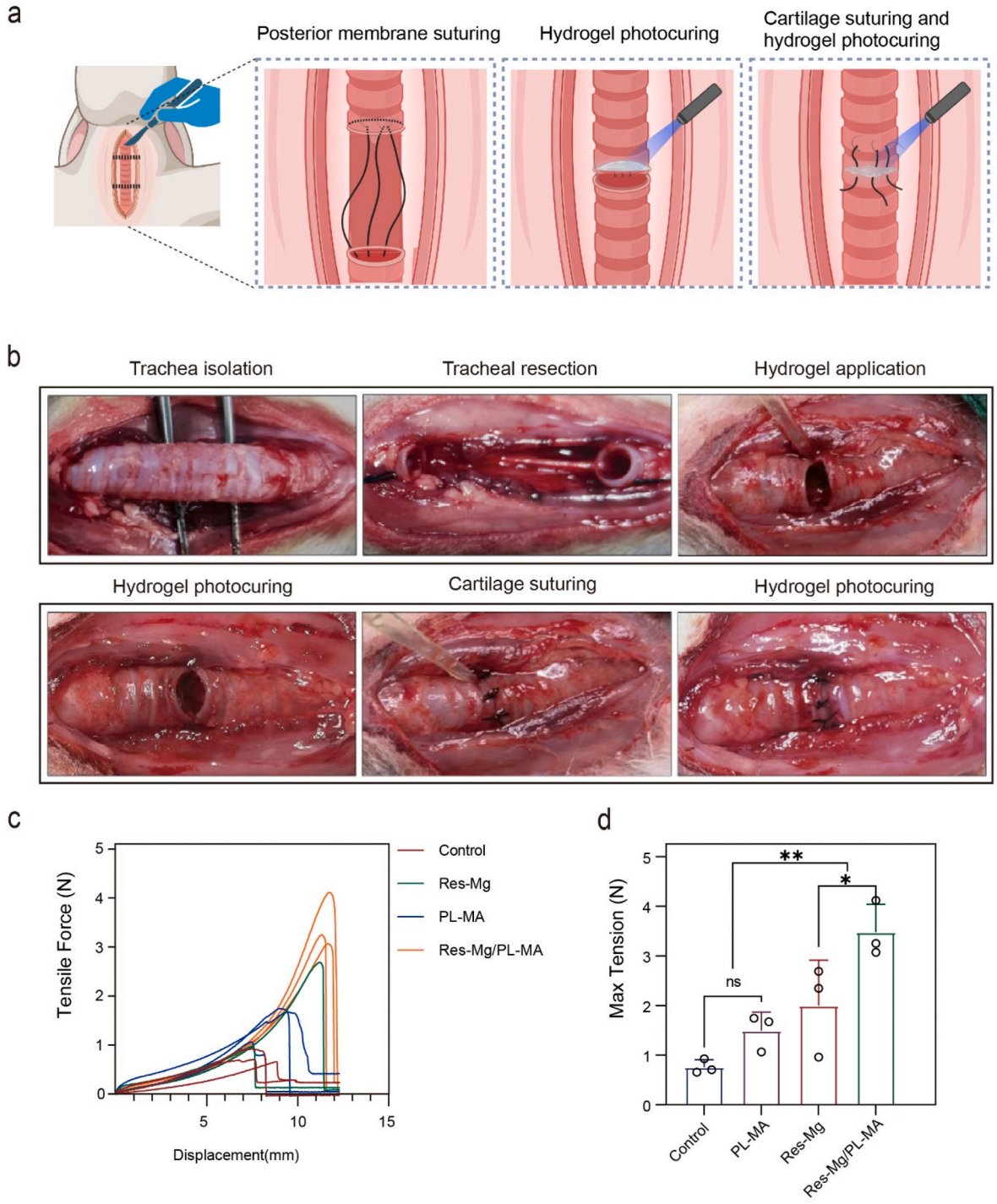

Fig. 4. a: Schematic illustration of the animal model construction. b: Representative intraoperative photographs of the animal model construction. c: The tension curves obtained from longitudinal tensile tests of rabbit tracheal anastomotic samples from different treatment groups. d: Maximum tensile strength of trachea from different treatment groups. Statistics were calculated with Student's t-test. *$p < 0.05$, **$p < 0.01$, ***$p < 0.001$, ****$p < 0.0001$ unless otherwise indicated. Data are presented as mean ± standard deviation (SD).

Resveratrol, a polyphenolic compound, has garnered significant attention in recent years due to its well-documented anti-inflammatory, wound healing, and anti-scarring properties [20]. Research suggests that its wound-healing attributes are linked to its ability to promote VEGF and activate the AMPK pathway [21,22]. On the other hand, its anti-scarring effects are attributed to its inhibition of the TGF-β1/Smad signaling pathway and the activation of SIRT1 [23,24]. In our screening of clinically relevant polyphenolic compounds, we found that resveratrol displayed the highest potential for suppressing TGF-β1 expression and augmenting VEGF expression in a trachea-derived fibroblast model. TGF-β1 serves as a crucial differentiation signal for fibroblasts, playing a pivotal role in their biological functions. Although our data showed that resveratrol did not significantly inhibit the proliferation of fibroblasts, their biological functions might be attenuated, as our experimental results demonstrated the inhibitory effect of resveratrol on granulation tissue proliferation, potentially achieved by suppressing TGF-β1 in fibroblasts to reduce collagen production.

Despite these established effects, the role of resveratrol in the context

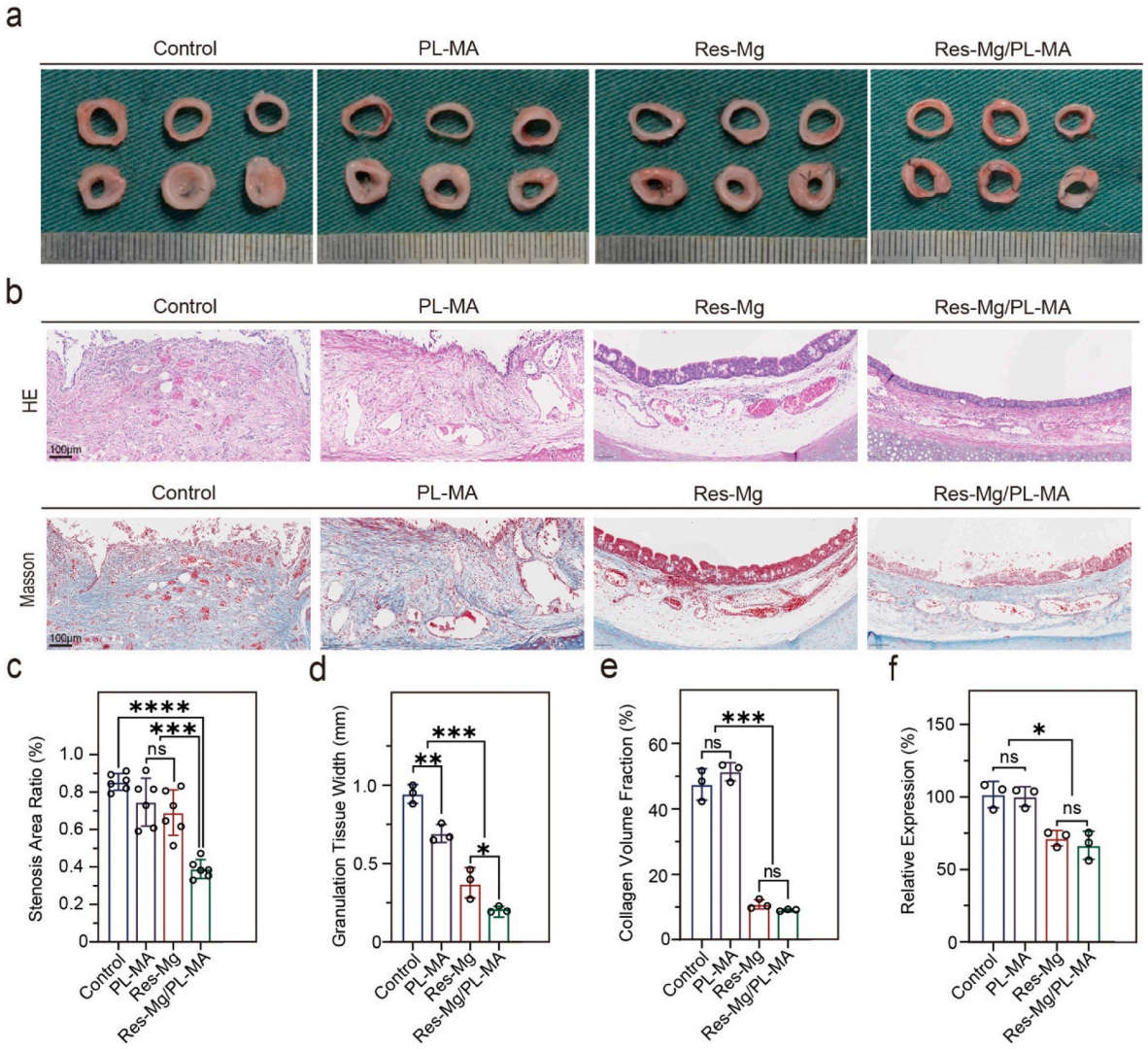

Fig. 5. a: Images depicting tracheal anastomosis sections from the indicated treatment groups, collected two weeks post-treatment. The two tracheal sections in the same image are obtained from a single rabbit. The upper panel showcases sections from a normal tracheal segment adjacent to the stenosis, while the lower panel displays sections from a segment where stenosis occurred. The normal tracheal segment serves as a reference for comparison. b: Masson and H&E staining of the tracheal anastomosis sections from different treatment groups. c: Percentage of the narrowed area in the tracheal anastomosis sections among the different treatment groups. d: thickness of the granulation tissue among the different treatment groups. e: collagen volume fraction (CVF) content among the different treatment groups. f: Relative expression levels of TGF-β1 in different treatment groups as determined by qRT-PCR. Statistics were calculated with Student's t-test. *$p < 0.05$, **$p < 0.01$, ***$p < 0.001$, ****$p < 0.0001$ unless otherwise indicated. Data are presented as mean ± standard deviation (SD).

of repairing tracheal anastomoses has remained unexplored. It's noteworthy that while some studies indicate its broad-spectrum antibacterial properties are effective in reducing skin wound infections, we did not observe such antibacterial activity at the sustained release concentrations in our tracheal anastomosis models [25]. This may be due to the local tissue release not reaching inhibitory concentrations. Additionally, resveratrol's role in stimulating SIRT1 results in the inhibition of fibroblast-to-myofibroblast transformation [26]. The observed increase in α-SMA expression in the Res-Mg and Res-Mg/PL-MA groups may be related to the effects of magnesium ions [27].

As previously mentioned, the primary hurdles associated with the utilization of resveratrol are its limited water solubility and restricted tissue bioavailability. To address this, several drug delivery systems have been developed to enhance its controlled release within local tissues. For instance, Gokce et al. devised resveratrol microcapsules for wound healing in diabetic mice [28]. Zhu et al. encapsulated resveratrol in mesoporous silica nanoparticles to improve its release kinetics [29]. The utilization of a liposome-chitosan gel as a drug carrier has also demonstrated promising outcomes across various disease models [30,31]. Our engineered Res-Mg metal-polyphenol network not only provides controlled release and tissue compatibility but also harnesses the wound-healing properties of magnesium ions. Additionally, the photosensitive nature of PL-MA allows for adaptable application to specific locations, catering to the intricacies of tracheal surgery.

The anti-tumor properties of resveratrol have become an increasingly explored area of research [32,33]. In NSCLC cell lines, studies have indicated that resveratrol can impede the activity of several NSCLC and induce apoptosis [34], findings that align with our own observations. Ma et al. have proposed that resveratrol can enhance the inhibitory effects of cisplatin on cancer cell proliferation [35], suggesting its potential broader application in cancer chemotherapy. Our biocompatibility experiments demonstrate that resveratrol at our experimental concentrations does not inhibit tracheal epithelial cells and fibroblasts. However, our anti-tumor experiments indicate significant inhibition of some but not all NSCLC cell lines by resveratrol. These observations were supported by previous evidence, demonstrating that the anticancer

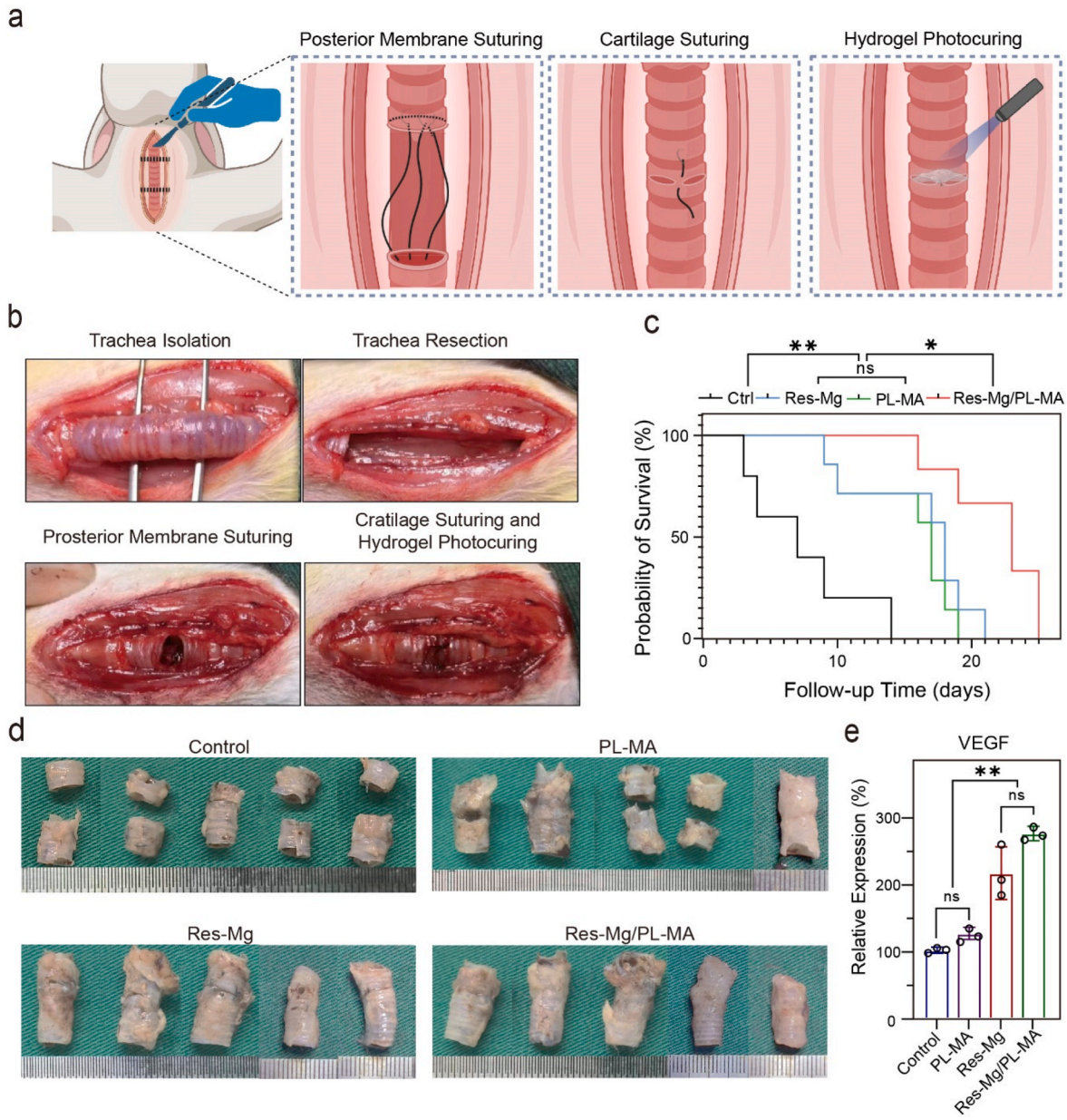

Fig. 6. a, b: Schematic representation and photographs of the animal model construction. c: Survival curves of rabbits from different treatment groups. d: Photographs of the tracheal anastomotic site and its surrounding segments obtained from different treatment groups of rabbits. e: Relative expression levels of VEGF in different treatment groups as determined by qRT-PCR. Survival significance is calculated using log-rank test. *$p < 0.05$, **$p < 0.01$, ***$p < 0.001$, ****$p < 0.0001$ unless otherwise indicated. Data are presented as mean ± standard deviation (SD).

effect of resveratrol selectively targets tumor cells primarily through the redox and metabolic differences between tumor and normal cells [36, 37]. Polyphenolic compounds can selectively target tumor cells by generating reactive oxygen species (ROS) through various mechanisms, thus mediating apoptosis in tumor cells [38]. Additionally, these compounds can target multiple cancer-related molecular dependencies, such as PI3K/Akt/mTOR, STAT3, MAPK, NF-κB, p53, thereby contributing to their selective anticancer properties [39].

Tracheal malignancy is a strong indicator for surgical intervention, accounting for half of all cases requiring tracheal surgery. ACC is the most prevalent histological subtype among tracheal malignant tumors [18]. While achieving negative margins in the surgical treatment of highly invasive tracheal ACC poses a considerable challenge, no evidence has yet demonstrated the effects of resveratrol on tracheal tumors. Our study not only reveals that resveratrol suppresses airway tumor cells in 2D culture but also demonstrates its efficacy in tracheal PDO models, which closely simulate real-world clinical scenarios [40].

The innovatively designed hydrogel adeptly amalgamates poly L-lysine gel with magnesium ions and resveratrol, optimizing their therapeutic efficacies in tracheal surgical wound contexts. The PL-MA gel serves to potentiate the local antibacterial kinetics of resveratrol, strategically mitigating infection-driven inflammatory surges. Concurrently, both resveratrol and magnesium ions, through augmented VEGF expression, spearhead angiogenesis. Their orchestrated release from the meticulously constructed metal-polyphenol network showcases a synergistic prowess, pivotal for microvascular re-establishment and expedited anastomotic healing. Furthermore, resveratrol's precise modulation of macrophage-mediated inflammation, coupled with its targeted inhibition of cardinal fibrogenic pathways, establishes a robust defensive front against anastomotic granulation and scar-mediated constriction. Collectively, empirical evidence underscores the substantial potential of the Res-Mg/PL-MA hydrogel in tension mitigation,

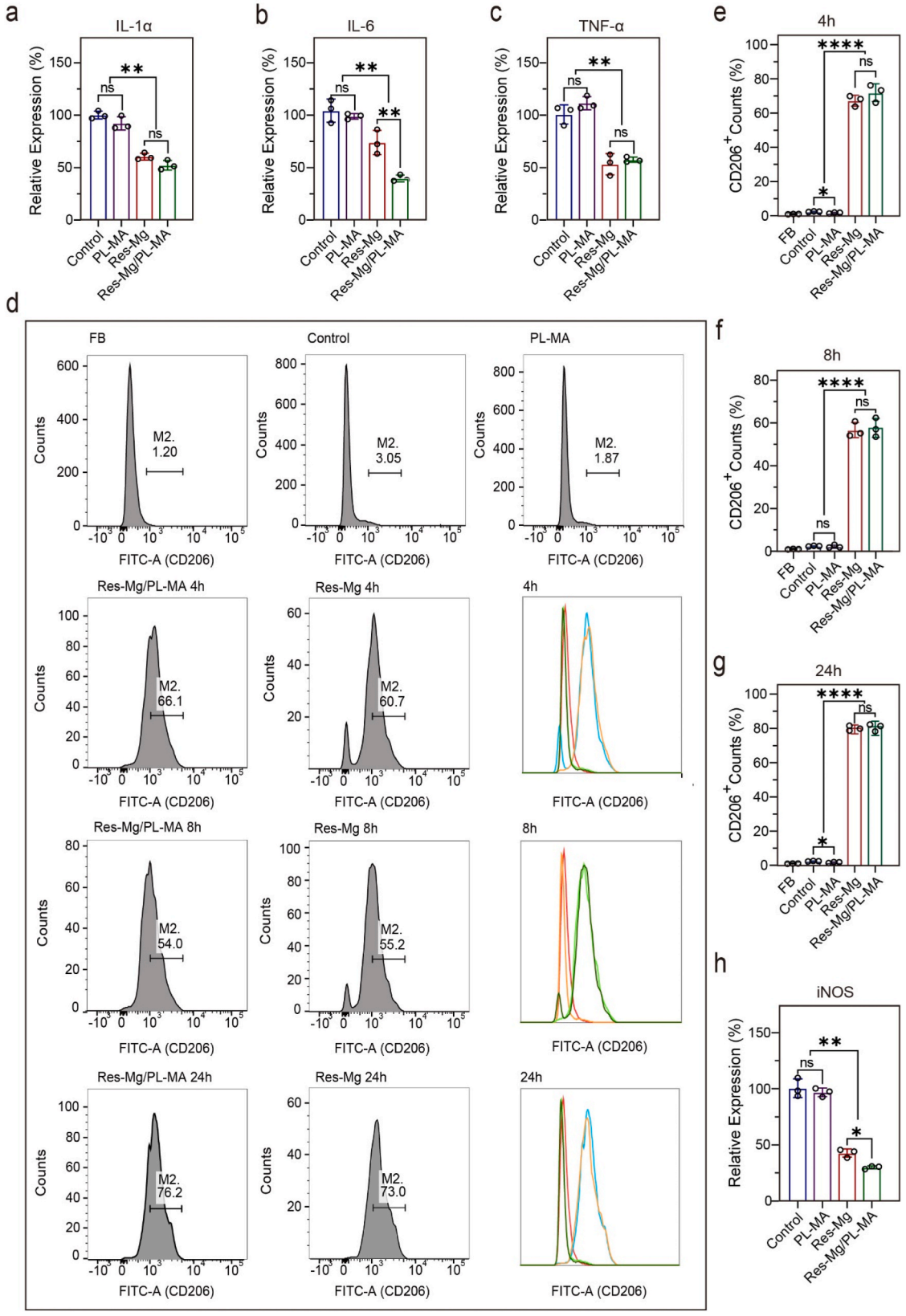

Fig. 7. a, b, c: Relative expression levels of IL-1α, IL-6, and TNF-α in different treatment groups as determined by qRT-PCR. d–g: The histogram and quantitative analysis depict the proportion of $CD206^{+}$ macrophages among different treatment groups, evaluated at 4-h, 8-h and 24-h intervals using flow cytometry. h: Relative expression levels of iNOS in different treatment groups as determined by qRT-PCR. Statistics were calculated with Student's t-test. *$p < 0.05$, **$p < 0.01$, ***$p < 0.001$, ****$p < 0.0001$ unless otherwise indicated. Data are presented as mean ± standard deviation (SD).

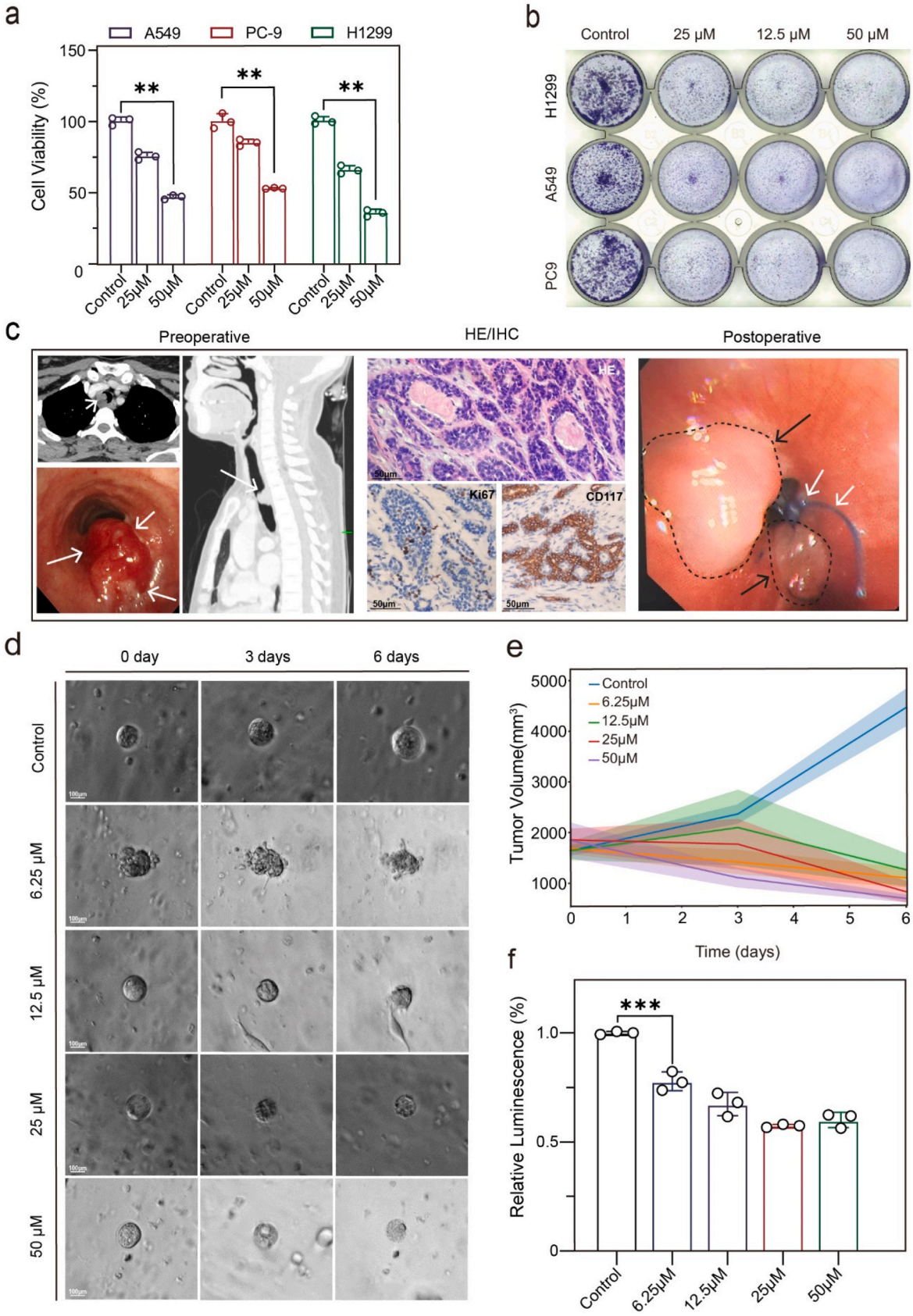

Fig. 8. a: Effects of different concentrations of resveratrol on the viability of various NSCLC cell lines. b: Colony formation photographs of the three sensitive cell lines. c: Preoperative CT images and bronchoscopic photos of the patient with PDO, as well as Postoperative tumor pathological section and bronchoscopic photos d: Images of tracheal tumor organoids after resveratrol treatment at different time points. e: Growth curves of organoids after resveratrol treatment. f: Cell viability of organoids detected by the ATP assay. Statistics were calculated with Student's t-test. *$p < 0.05$, **$p < 0.01$, ***$p < 0.001$, ****$p < 0.0001$ unless otherwise indicated. Data are presented as mean ± standard deviation (SD).

angiogenic facilitation, granuloma growth attenuation, bacterial infection counteraction, and malignant airway tumor suppression. This paves the way for a transformative paradigm in the clinical stewardship of anastomotic sites post-tracheal interventions.

Our study has several limitations to consider. Anastomotic complications typically result from the interaction of multiple factors, and our model primarily simulates localized foreign body and tension dynamics following resection, which may not fully replicate real-world clinical scenarios. Additionally, although our *in vitro* findings are promising, the anti-tumor potential of our hydrogel requires further examination through *in vivo* orthotopic models.

4. Conclusion

The meticulously designed Res-Mg/PL-MA hydrogel, by adeptly combining the strengths of poly L-lysine gel, magnesium ions, and resveratrol, offers a comprehensive and promising therapeutic strategy for the management of anastomotic sites post-tracheal surgery. It demonstrates significant efficacy in both *in vitro* studies and animal model evaluations, effectively mitigating infection-induced inflammation, promoting the polarization of anti-inflammatory macrophages, impeding excessive granulation tissue growth, particularly addressing scar-induced stenosis at the anastomotic site. Notably, this hydrogel enhances the expression of VEGF, facilitating vascular regeneration and expediting wound healing. Overall, it exhibits outstanding capabilities in tension alleviation, angiogenesis promotion, granuloma inhibition, bacterial infection intervention, and malignant airway tumor suppression, signifying its potential to be a groundbreaking therapeutic tool in the clinical management of tracheal surgical wounds.

5. Experimental methods

Materials and Cell Culture: Poly-L-lysine Methacryloyl (PL-MA) was purchased from Engineering for Life Company (Suzhou, China). Resveratrol was obtained from Aladdin (Shanghai, China). Cells were cultured in RPMI-1640 medium (Sigma-Aldrich, St. Louis, MO, USA) supplemented with FBS (Life Technologies, Grand Island, NY, USA) and 1 % penicillin/streptomycin (Sigma-Aldrich). The culturing conditions were 37 °C with 5 % CO2.

Preparation of Res-Mg Hydrogel: Our Res-Mg material was synthesized using the traditional method. 0.5g of MgCL2 and 2.28g of resveratrol powder were dissolved in 25 mL ethanol and stirred. While stirring, a 0.1 mM KOH solution was added dropwise to adjust the pH to 8, and the mixture was incubated at room temperature for 24h. The resultant product was obtained by centrifugation at 12000 rpm, 4 °C for 15 min, followed by two ethanol washes. For the synthesis of Mg-Res-Mg/PL-MA hydrogel, 5 mg of Res-Mg and 0.15 g of PL-MA were dispersed in 500 μL of H2O containing 0.25 % photoinitiator LAP, and ultrasonicated at 4 °C for 30 min to achieve dispersion.

In vitro Drug Release: Sample synthesis: 3.8g of gallic acid and 1g of MgCl2 were dissolved in 50 mL of water. The pH was adjusted to 8.0 by adding 10 mM KOH. The mixture was stirred at 140 °C for 24 h. It was then centrifuged at 12000 rpm and 4 °C for 15 min, followed by washing twice with water16. 5 mg of Res was dispersed in 500 μL of H2O containing 0.25 % photoinitiator LAP with PL-MA, while GA-Mof was dispersed with PL-MA in another 500 μL of H2O containing the same photoinitiator. Both dispersions were sonicated at 4 °C for 30 min to achieve dispersion. Subsequently, exposure to 405 nm light solidified the Res/PL-MA and GA-Mof/PL-MA independently.

30 mg each of Res-Mg/PLMA, Res-Mg, Res/PL-MA, and GA-Mof/PL-MA were added to 10 mL of PBS and thoroughly mixed at 37 °C. At different time points (0, 4, 8, 12, 24h, 3d, 4d, 5d, 6d, 7d), 15 μL of supernatant was collected and supplemented with PBS to equal volumes. Absorbance at 280 nm was measured using a UV spectrophotometer (UV-5100, Shanghai Metash Instruments Co., Ltd., Shanghai, China).

Cell Viability Assay and Colony Formation: Cells were seeded in 96-well plates (1500–3000 cells/well) and cultured for 24h. After 72h of drug treatment, viability was assessed using the Alkaline Phosphatase Assay Kit (ab83367; Abcam, Cambridge, UK), as we previously described [41–44]. For the colony formation assay, cells were seeded at a density of 104 cells/well in 12-well plates. Based on the growth rate of cells, drug treatment was administered for 72 h or longer, followed by crystal violet staining. After crystal violet staining, 1 mL of methanol was added to each well of the 12-well plate. The plate was then agitated using a pipette for thorough mixing. Quantification of the colony clone results was achieved by measuring the absorbance at 540 nm using a spectrophotometer.

Flow Cytometry (FC): After drug treatment, cells were labeled with CD206 (MMR) antibody (BioLegend, Inc. San Diego, CA, USA) following the manufacturer's instructions. Analysis was performed using a Cantoll flow cytometer (BD Bioscience) and data was analyzed using FlowJo V10 (Tree Star, Inc. Ashland, OR, USA).

qRT-PCR: Total RNA was extracted using the RNeasy kit (74106; Qiagen, Hilden, Germany). Complementary DNA (cDNA) was synthesized using the High-Capacity cDNA Reverse Transcription Kit (4368814; Applied Biosystems, Foster City, CA, USA) according to the manufacturer's instructions. PCR was conducted using specific primers (sangon biotech, Shanghai, China) on a QuantStudio Dx Real-time PCR instrument (Thermo Fisher), with GAPDH serving as the endogenous normalization control.

Animal Model: 56 New Zealand white rabbits (3 months old, male, weighing 2.5–3.0 kg, from Shanghai Jiao Tong University's Agriculture and Life Experimental Facility Co., Ltd.) were used in this study. The study complied with the guidelines and protocols approved by the Institutional Animal Care and Use Committee.

Granulation Tissue Proliferation Model: After anesthetizing the rabbit, the trachea is isolated. Half of the cervical segment of the trachea (approximately 2.5 cm) is excised, and the tracheal posterior membrane is sutured with 6-0 silk sutures. Gel is applied using a pipette, followed by a preliminary photo-curing using 405 nm UV light for 5 s. The tracheal cartilage is then sutured with 6-0 silk sutures, gel is reapplied, and it's photo-cured again for 10 s.

Anastomosis Separation Model: After anesthetizing the rabbit, the trachea is isolated. Half of the cervical segment of the trachea (approximately 2.5 cm) is excised, and the tracheal posterior membrane is sutured with 6-0 silk sutures. Gel is applied using a pipette, followed by a preliminary photo-curing using 405 nm UV light for 5 s. A suture is placed in the center of the cartilage, leaving two potential fistulas on either side. Gel is applied to the potential fistula sites on both sides and is photo-cured for 10 s.

Histological Study: Hematoxylin and Eosin (H&E) and Masson's Staining: Tracheal tissues from the anastomosis site were collected post-euthanasia and fixed in 4 % paraformaldehyde for 24h. The tissues were then dehydrated, embedded in paraffin, and sectioned at 5 μm for H&E and Masson's staining.

Immunohistochemistry: Rabbit tracheal tissue samples were stained for CD31 and α-SMA, with antibodies sourced from Servicebio (Wuhan, Hubei, China).

Histological Quantification: Quantitative analysis of immunohistochemistry and Masson's staining was conducted using the open-source software Qupath and ImageJ. Within Qupath, the built-in wand tool was employed for semi-automatic selection of granulation tissue regions and cell detection. The object classifier was used to automatically distinguish between positive and negative cells and calculate their proportions [45–48]. ImageJ's Threshold function was utilized to differentiate collagen fibers from other tissues and to compute the collagen volume fraction.

Patient Derived Organoid Culture: Primary ACC tumor cells from patients were harvested and resuspended, then seeded onto a 48-well cell culture plate containing matrix gel. Each well was supplemented with 300 μl of lung cancer organoid culture medium (Innovation Biotech IB-LuCOM-001, Tianjin, China) containing 10 μg/mL DNAse and 10.5 μM

Y-27632. The medium was refreshed every 72 h. Once the organoids were formed, they were treated with varying concentrations of the drug for 72 h, after which the drug was withdrawn. The growth status of the organoids was documented every three days using a laser confocal microscope (Zeiss, Oberkochen, Baden-Württemberg, Germany).

ATP Luminescent Cell Viability Assay: The ATP assay kit was obtained from Promega Biotech (Beijing, China). A 1:1 ratio of CellTiter-Glo buffer was added to each well. After shaking for 2 min, the mixture was allowed to stand for 10 min. Cell viability was then determined by measuring the luminescence intensity.

Statistical Analysis: Data are presented as mean ± standard deviation. Analysis was conducted using GraphPad Prism 7.0 (GraphPad Software, Inc., San Diego, CA, USA). Two groups were compared using the *t*-test, while one-way ANOVA was used for comparing three or more groups. Survival analysis was conducted using the Log-rank (Mantel-Cox) test. Differences with $p < 0.05$ were considered statistically significant.

Ethics approval and consent to participate

All experimental procedures were conducted in accordance with institutional guidelines for the care and use of laboratory animals and protocols, which were approved by the Animal Care and Use Committee of Shanghai Chest Hospital.

Consent for publication

All medical imaging and pathological data mentioned in the article have been obtained with the informed consent of the patient.

Availability of data and materials

The authors declare that the main data supporting the findings of this study are available within the article and its Additional file Information. Extra data are available from the corresponding author upon request.

Funding

This work was supported by the Basic Foundation Program for Youth of Shanghai Chest Hospital (2021YNJCQ2 to H.Y), Shanghai Pujiang Program (22PJD068 to H.Y), the excellent talent program of Shanghai Chest Hospital (to F.Y), and the Innovative Research Team of High-level Local Universities in Shanghai (SHSMU-ZLCX20212302 to F. Yao).

CRediT authorship contribution statement

Yunxuan Jia: Conceptualization, Data curation, Formal analysis, Investigation, Methodology, Project administration, Resources, Software, Supervision, Validation, Visualization, Writing - original draft, Writing - review & editing. **Jingfeng Shi:** Software, Visualization, Writing - original draft. **Bowen Ding:** Funding acquisition, Investigation, Methodology, Validation, Visualization, Writing - original draft. **Liang Zhao:** Data curation, Formal analysis, Investigation, Methodology. **Ke Xu:** Data curation, Formal analysis, Investigation, Methodology. **Chuang Hu:** Data curation, Formal analysis, Investigation, Methodology, Writing - original draft, Writing - review & editing. **Weijiao Xu:** Resources, Software, Supervision. **Anshun Zhu:** Resources, Software, Supervision, Validation. **Haitang Yang:** Conceptualization, Data curation, Formal analysis, Funding acquisition, Investigation, Methodology, Project administration, Resources, Software, Supervision, Validation, Visualization, Writing - original draft, Writing - review & editing. **Xiansong Wang:** Conceptualization, Data curation, Project administration, Software, Supervision, Validation, Visualization, Writing - original draft, Writing - review & editing. **Feng Yao:** Data curation, Formal analysis, Funding acquisition, Validation, Writing - original draft, Writing - review & editing.

Declaration of competing interest

The authors declare that they have no known competing financial interests or personal relationships that could have appeared to influence the work reported in this paper.

Data availability

Data will be made available on request.

Acknowledgements

Not applicable.

Appendix A. Supplementary data

Supplementary data to this article can be found online at https://doi.org/10.1016/j.mtbio.2023.100938.

References

[1] G. Leschber, Thorac. Surg. Clin. 24 (1) (2014) 107.
[2] S. Sihag, C.D. Wright, Thorac. Surg. Clin. 25 (4) (2015) 499.
[3] H.G. Auchincloss, C.D. Wright, J. Thorac. Dis. 8 (Suppl 2) (2016) S160.
[4] S. Kim, et al., Semin. CardioThorac. Vasc. Anesth. 21 (4) (2017) 360.
[5] M. Sippel, et al., Thorac. Cardiovasc. Surg. 54 (1) (2006) 51.
[6] L.F. Tapias, et al., Eur. J. Cardio. Thorac. Surg. 57 (6) (2020) 1203.
[7] T. Oda, et al., J. Artif. Organs 14 (3) (2011) 245.
[8] B. Broussard, D.J. Mathisen, Ann. Cardiothorac. Surg. 7 (2) (2018) 293.
[9] G. Broughton 2nd, et al., Plast. Reconstr. Surg. 117 (7 Suppl) (2006) 1e.
[10] P. Simoni, B.J. Wiatrak, Laryngoscope 114 (2) (2004) 364.
[11] B.S. Quon, et al., Ann. Am. Thorac. Soc. 11 (3) (2014) 425.
[12] Z. Li, et al., Colloids Surf. B Biointerfaces 206 (2021), 111949.
[13] X. Wang, et al., Int. J. Biol. Macromol. 187 (2021) 91.
[14] P. Wang, et al., J. Nanobiotechnol. 20 (1) (2022) 259.
[15] P. Zhang, et al., Biomater. Sci. 11 (20) (2023) 6848.
[16] M. Yin, et al., ACS Nano 15 (11) (2021), 17842.
[17] Y. Gong, et al., ACS Nano 17 (22) (2023), 22355.
[18] H. Yang, et al., Ann. Thorac. Surg. 101 (1) (2016) 294.
[19] C.J. Mutrie, et al., Ann. Thorac. Surg. 91 (4) (2011) 1101.
[20] A. Hecker, et al., Int. Wound J. 19 (1) (2022) 9.
[21] P. Zhao, et al., Aging Cell 16 (5) (2017) 1083.
[22] S Khanna, et al., Free Radical Biol. Med. (2002) 33.
[23] A.L. Pignet, et al., Int. J. Mol. Sci. 22 (23) (2021).
[24] X.X. Zhai, et al., Cell Biochem. Biophys. 71 (3) (2015) 1267.
[25] M. Vestergaard, H. Ingmer, Int. J. Antimicrob. Agents 53 (6) (2019) 716.
[26] X.Z. Bai, et al., Br. J. Pharmacol. 173 (10) (2016) 1589.
[27] F. Yang, et al., Bioact. Mater. 26 (2023) 88.
[28] E.H. Gokce, et al., Eur. J. Pharm. Biopharm. 119 (2017) 17.
[29] W. Zhu, et al., Acta Biomater. 154 (2022) 212.
[30] M.W. Joraholmen, et al., Pharmaceutics 14 (6) (2022).
[31] R. Conte, et al., J. Funct. Biomater. (2) (2023) 14.
[32] B. Ren, et al., Cancer Lett. 515 (2021) 63.
[33] M. Annaji, et al., Cancer Rep. 4 (3) (2021) e1353.
[34] I. Lucas, H. Kolodziej, Planta Med. 81 (12/13) (2015) 1038.
[35] L. Ma, et al., Int. J. Oncol. 47 (4) (2015) 1460.
[36] T. Kiskova, M. Kassayova, Int. J. Mol. Sci. 20 (11) (2019).
[37] A. Niedzwiecki, et al., Nutrients 8 (9) (2016).
[38] C. Feng, et al., Macromol. Biosci. 23 (11) (2023), e2300167.
[39] D. Chuan, et al., J. Mater. Sci. Technol. 152 (2023) 159.
[40] S. Karkampouna, et al., Nat. Commun. 12 (1) (2021) 1117.
[41] H. Yang, et al., Oncogenesis 8 (9) (2019) 45.
[42] H. Yang, et al., Cell Death Dis. 9 (1) (2023) 55.
[43] T. Zhang, et al., Transl. Lung Cancer Res. 10 (4) (2021) 1857.
[44] H. Yang, et al., EBioMedicine 69 (2021), 103457.
[45] H. Yang, et al., EBioMedicine (2022) 84.
[46] H. Yang, et al., Theranostics 12 (7) (2022) 3104.
[47] H. Yang, et al., Theranostics 12 (1) (2022) 167.
[48] P. Bankhead, et al., Sci. Rep. 7 (1) (2017), 16878.

Abbreviations

Res: Resveratrol
MPN: Metal polyphenol network
Res-Mg: Metal-phenolic network made from magnesium ions and resveratrol
PL-MA: Poly-L-lysine Methacryloyl hydrogel
Res-Mg/PL-MA: Hydrogel prepared from magnesium ion-resveratrol metal-phenolic network and Poly-L-lysine Methacryloyl

CVF: Collagen volume fraction
ACC: Adenoid cystic carcinoma
NSCLC: Non-small cell lung cancer
PDO: Patient-derived organoid